



Numerical analysis of thermal comfort and air freshness generated by a multi-cone diffuser with and without lobed inserts

Ahmed Benabed, Amir Boulbair

► To cite this version:

Ahmed Benabed, Amir Boulbair. Numerical analysis of thermal comfort and air freshness generated by a multi-cone diffuser with and without lobed inserts. Journal of Building Engineering, 2022, 54, pp.104632. 10.1016/j.jobr.2022.104632 . hal-04497957

HAL Id: hal-04497957

<https://hal.science/hal-04497957>

Submitted on 22 Jul 2024

HAL is a multi-disciplinary open access archive for the deposit and dissemination of scientific research documents, whether they are published or not. The documents may come from teaching and research institutions in France or abroad, or from public or private research centers.

L'archive ouverte pluridisciplinaire **HAL**, est destinée au dépôt et à la diffusion de documents scientifiques de niveau recherche, publiés ou non, émanant des établissements d'enseignement et de recherche français ou étrangers, des laboratoires publics ou privés.



Distributed under a Creative Commons Attribution 4.0 International License

Numerical analysis of thermal comfort and air freshness generated by a multi-cone diffuser with and without lobed inserts

Ahmed Benabed¹, Amir Boulbair²

¹Departement of Mechanical and Environmental Engineering, ESTACA, Paris-Saclay Campus, 78180, Montigny-le-Bretonneux, France.

²Univ. Polytechnique Hauts-de-France, LAMIH, CNRS, UMR 8201, F-59313 Valenciennes, France

Abstract

In this work, a numerical investigation using Ansys Fluent software is performed to study the flow pattern, the indoor thermal comfort, and the air freshness generated in a full-scale ventilated office room occupied by a sitting occupant. The performance of a multi-cone ceiling diffuser equipped with lobed inserts is assessed and compared with a traditional multi-cone ceiling diffuser. The indoor thermal comfort is evaluated using the predicted percentage of dissatisfaction (*PPD*) and the draft rate (*DR*) indicators. To assess the air freshness inside the office room, the mean age of air (*MAA*) is evaluated. After validating the simulation, the effect of the supply flow rate on the airflow pattern, the thermal comfort, and the air freshness, are investigated. Velocity contours show that recirculation zones in the domain result from the interaction between the supplied air and the thermal plume above the occupant's head. The statistical analysis of *PPD* and *DR* reveals that - depending on the supply flow rate - lobed inserts reduce the thermal dissatisfaction and the draft effect in the occupied zone. However, in terms of *MAA*, the lobed inserts reduce the air freshness slightly in the vicinity of the occupant's head.

Key words: air freshness, mean age of air, thermal comfort, ceiling diffuser, lobed inserts

1. Introduction

In modern technological societies, people spend more than 90% of their time indoors (homes, workplaces, ...). Therefore, thermal comfort and indoor air quality in these environments are becoming increasingly important as they are fundamental to the well-being of occupants. It has been proven that heating, ventilating, and air-conditioning (HVAC) systems are necessary to ensure comfortable and healthy indoor environment [1,2]. However, by looking at the distribution of energy consumption in a conventional building, it can be noticed that heating and ventilation systems consume the largest part of the operational energy of the building [3]. Therefore, it has become crucial to find efficient and low-cost ventilation configurations.

The design of an effective air distribution system is based primarily on its ability to provide good air quality and an adequate level of thermal comfort in the occupied zone [4, 5]. The latter is defined as the region normally occupied by people within a space generally considered to be between the floor and 1.8 m level above the floor and 0.6 m from all vertical walls [6]. Most air distribution systems are based on mixing ventilation using ceiling diffusers, wall-mounted diffusers, displacement ventilation by means of wall-mounted low velocity diffusers, or ceiling-mounted textile terminals. Several research studies have been carried out to identify the requirements of each system, their advantages, and their inconveniences, and to select the most appropriate system for the various configurations. Nielsen et al. [7] show that an air distribution system with ceiling-mounted air terminal units can guarantee comfortable conditions of velocity and temperature at the same or at slightly higher loads as can be obtained by the other distribution systems. Based on the velocity decay measurement, Chuah et al. [8] and later Shakerin and Miller [9] showed experimentally that with a vortex diffuser, more ambient air is mixed into the occupied zone. Hu [10] investigated experimentally flow patterns and

thermal comfort generated by ceiling flush-mounted diffusers in cooling mode. They showed that both the vortex diffuser and the nozzle-type diffuser can provide a very good indoor thermal comfort compared with that provided by the multi-cone round diffuser. Aziz et al. [11] investigate experimentally and numerically airflow characteristics, thermal comfort, and air freshness in a ventilated room alternately equipped with vortex, round, and square ceiling diffusers. The authors evaluate the performance of each diffuser using the velocity decay coefficient. Contrary to the previously discussed works [8,9,10], the performance of the round diffuser is 2.6 times greater than that of the vortex diffuser and is nearly the same as for the square diffuser. Results of Aziz et al. [11] show that the saved energy by vortex diffuser is 1.5 times lower than that achieved by square or round diffusers. The differences between their results and those of [8,9,10] can be attributed to the jet's characteristics at the diffuser's outlet. Indeed, the jet is vertical in [11] and attached to the ceiling in [8,9,10]. Aziz et al. [11] show also that swirly angle has a significant impact on the jet throw, therefore on the diffuser's efficiency. This result has been previously demonstrated in a numerical work conducted by Sajadi et al. [12].

An innovative and passive concept has been suggested, in which the efficiency of air mixing system can be improved without replacing the diffuser. These techniques consist in introducing corrugated devices called lobed nozzles/mixers into the diffuser. In the aforementioned, the boundary layers of the supply air are sheared locally by the corrugations. Consequently, vortex structures are created which increase the auto-induction of the supplied air, thus, increasing air mixing. This device was first validated in the aeronautics and aerospace fields. For example, to reduce take-off jet noise and fuel consumption on some commercial aircraft engines [13,14] or to enhance the mixing process of the high temperature and the high-speed gas plume from the air-engine with ambient cold air [15,16]. In building applications, Nastase et al. [17] have shown experimentally in isothermal conditions that; jet flows from rectangular air diffusion grilles equipped with lobed ailerons ensure higher mixing in a room than baseline jet flows from classical rectangular air diffusion grilles with straight ailerons. The authors suggest lobed ailerons as a solution to ensure more uniform flows and to reduce thermal discomfort and draught sensation in indoor environments. Bragança et al. [18] investigated experimentally the airflow pattern and evaluated the thermal comfort in terms of predicted percentage of dissatisfaction (*PPD*) and draft rate (*DR*) indices inside a climate chamber by a ceiling round diffuser in summer conditions. The effect of lobed inserts introduced into the diffuser has been evaluated. According to the authors, the analysis reveals an improvement in thermal comfort in the lobed diffuser case compared to the conventional diffuser case, and this was achieved without a significant increase in pressure loss and noise. This result has been confirmed later in the same climate chamber using the same ceiling round diffuser in winter conditions [19].

The effectiveness of the lobed inserts in improving thermal comfort has been previously studied experimentally. However, the evaluation of these devices has been usually carried out according to the comfort indices without taking into consideration the air freshness. The latter is a crucial parameter for the evaluation of ventilation system efficiency. Also, the need for good levels of air freshness has been promoted recently after the spread of the COVID-19 in the world [20] and the demonstration that its transmission route had a significant impact on the number of infections [21]. Furthermore, the effectiveness of the lobed inserts in the context of indoor thermal comfort and air freshness was not investigated using computational fluid dynamics (CFD). One benefit of the latter is the computation of the full flow field within the entire domain, which offers a complete picture of thermal comfort and air freshness. However, in experimental techniques, variables are assessed in a limited number of points. The aim of the present study is therefore to assess and explore, using the CFD approach, the performance of lobed inserts in ensuring good thermal comfort and air freshness (in cooling mode) inside an office room compared to a classical multi-cone diffuser. The assessment of global thermal comfort was based on the *PPD* and *DR* indices considering a sitting occupant, wearing working clothing, and having sedentary activity. The air freshness was assessed via the mean age of air *MAA* criteria. The latter is a valuable tool for evaluating the performance of ventilation systems.

2. Methods

2.1 Geometry and meshing

The general layout of the computational domain consists of a duct with 0.08 m radius and 1.6 m long, a three-cone round diffuser, and 3.47 m × 3.47 m × 2.5 m office room (Figure 1(a)). Dimensions of the computational domain were constructed according to the real dimensions of the experimental chamber presented by Bragança et al. [18]. In the latter, the inside faces of the climatic chamber were thermally controlled. Their configuration also allows the control of mean ambient temperature and the initial flow rate. The seated manikin used in the experimental study has 8 heated parts and total power of 81 W, which leads to a mean surface temperature of 32 °C. Measurement of air velocity was carried out using 2D2C Dantec Dynamics PIV system. Air temperature in the occupied zone was measured using thermocouples at 64 points.

The present study was conducted in two cases: in case 1, the air was supplied through a ceiling round diffuser, and in case 2, the air was supplied through the same round diffuser equipped with lobed inserts. In the following, case 1 and case 2 will be referenced as CD (conventional diffuser) and CDLI (conventional diffuser with lobed insert) respectively. Geometry and detailed profile of the round diffuser and the lobed inserts are shown in Figure 2. The room was occupied by one simplified sitting occupant positioned in the middle of the room (Figure 1(b)). As reported in the literature [22,23], a simplified geometry of the human body is sufficient when the interest deals with the global airflow pattern and thermal comfort criteria. Finally, no obstacles, such as furniture, were introduced inside the CFD office room. All geometries were built using SolidWorks software.

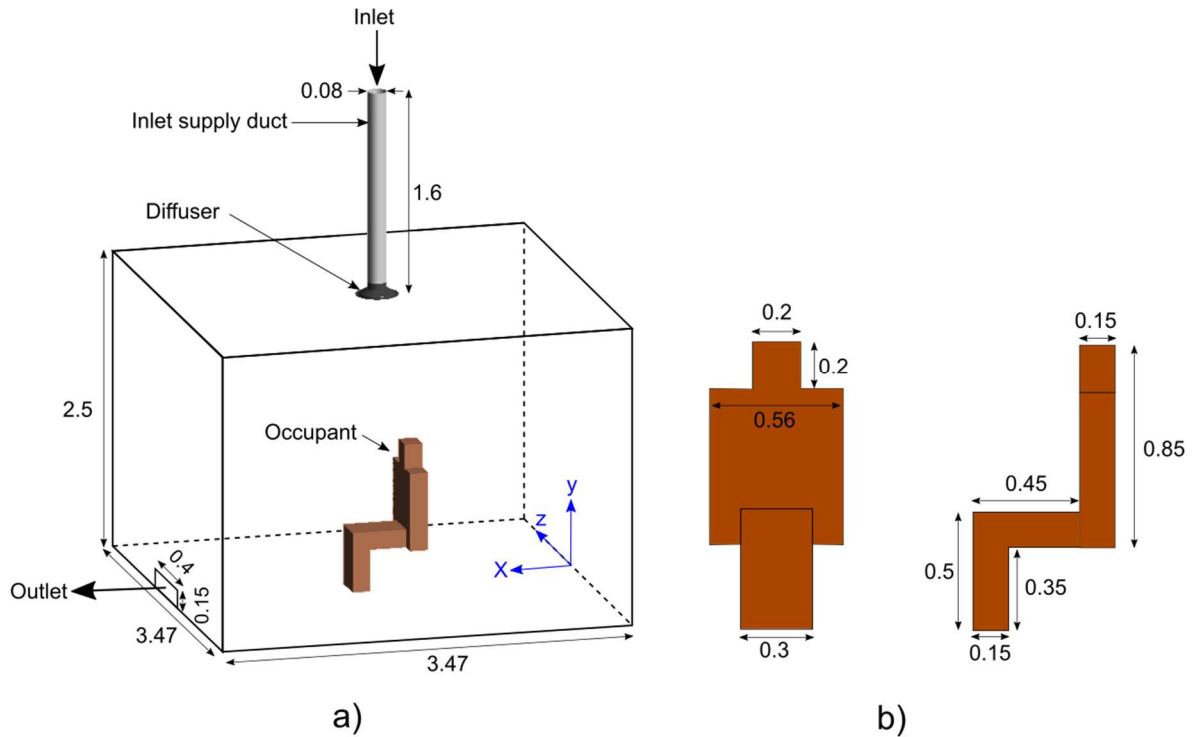


Figure 1. a) The computational domain dimensions, b) The sitting occupant dimensions.

Creating a high-quality mesh is one of the most critical factors that must be considered to ensure simulation accuracy. In the present work, the two main difficulties during the meshing step were (1) the complex geometry of the diffuser, which becomes more complex when adding lobed inserts, (2) the considerable difference between the diffuser and the office dimensions, and (3) the presence of the occupant in the domain. These may lead to a large mesh aspect ratio and/or skewness in the region near the diffuser, which causes convergence problems and affects the results' accuracy. To avoid these problems; first, the diffuser and the zone around the occupant were meshed using tetrahedral cells, whereas the duct and the office were meshed using cartesian hexahedra cells (see Figure 3). Second,

two transition zones with tetrahedral cells were created between the duct and the diffuser, and between the diffuser and the room. The cell sizes in the vicinity of the solid surfaces (walls, occupant) as well as the supply and the exhaust were refined using the inflation option with $y^+ < 1$.

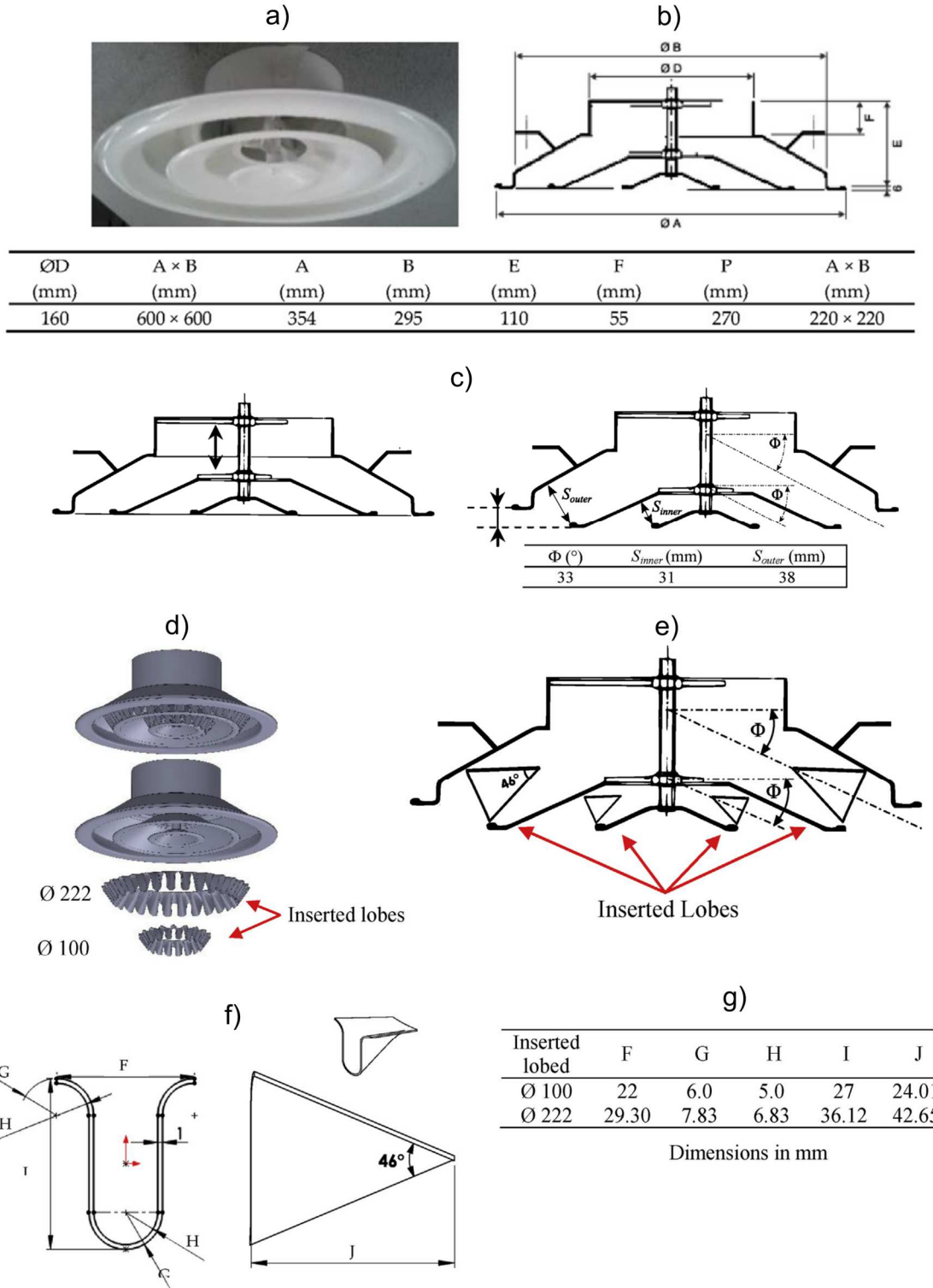


Figure 2. (a, b) Conventional diffuser (CD) and its dimensions; (c) Control-setting of jet behavior - double-headed arrow (left) indicates the movement up/down of the inner cones, the two arrows (right) indicate the position of inner cones for radial jet generation; (d, e) Mounting of the lobed inserts into the CD, (f, g) Geometry details of the lobed inserts [18].

The commercial CFD software Ansys Fluent was used to study and simulate the airflow characteristics, temperature, and *MAA* distribution patterns inside the office room. The airflow used in the simulation is considered as steady, incompressible, and turbulent. Beside the averaged Navier-Stokes equations, the energy equation was also solved to calculate air temperature fields inside the office room. The Simple algorithm was used for coupling pressure and velocity. The second-order upwind differencing scheme was chosen as the discretization scheme for the convection terms of each governing equation. A user-defined scalar (UDS) was used for solving *MAA*. Once the airflow simulations had been carried out, *PPD* and *DR* indicators - not available in Fluent - were calculated using a user-defined function (UDF).

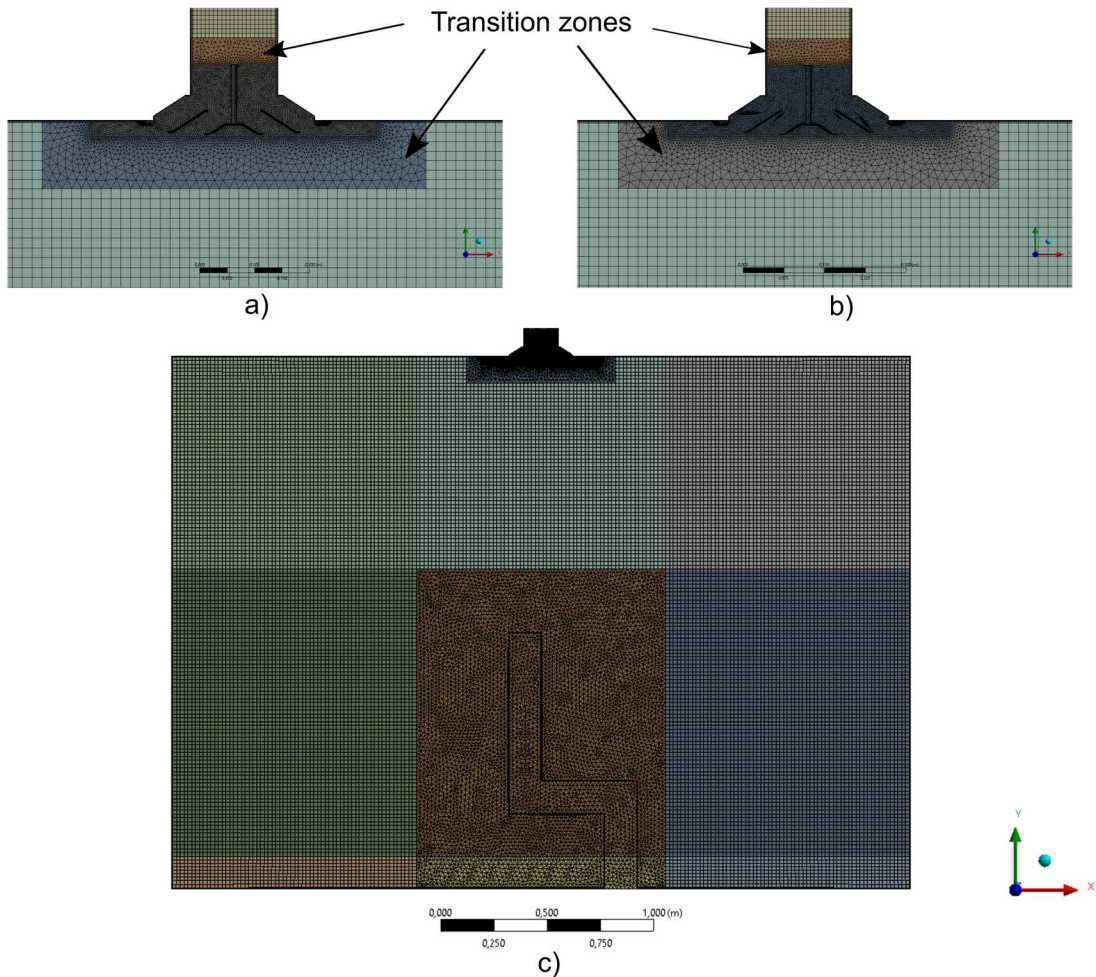


Figure 3. Mesh in a-b) the vicinity of the diffusers, c) the office.

2.2 Air freshness and thermal comfort indices calculation

In this study, air freshness and thermal comfort parameters have been defined as follows:

2.2.1 Mean age of air evaluation

The *MAA* was used as an indicator of air freshness. The *MAA* is defined as the average age of the air in a certain location. It is obvious that local *MAA* values will significantly increase if part of the air circulates for a long time inside the room, which depends strongly on the effectiveness of the ventilation system [24].

In this study, *MAA* has been solved as a steady additional transport scalar following Equation (1) [25,26]:

$$\frac{\partial}{\partial x_i} \left(\rho u_i \tau - \left(2.88 \times 10^{-5} \times \rho + \frac{\mu_{eff}}{0.7} \right) \frac{\partial \tau}{\partial x_i} \right) = S_\tau \quad (1)$$

where

- τ : the *MAA* (s).
- ρu_i : the mass flow rate ($\text{kg} \cdot \text{m}^{-2} \text{s}^{-1}$).
- $2.88 \times 10^{-5} \times \rho + \frac{\mu_{eff}}{0.7}$: is the diffusion coefficient of the *MAA*. A value of 2.88×10^{-5} means a constant laminar viscosity; this may be appropriate only for air at a constant temperature of 20 °C. Though, if air temperature decreases from 20 °C to 0 °C, the difference in laminar viscosity value will reach over 10%. This variation could be significant only in areas with laminar flow regime. However, for turbulent flows, it will have a poor effect because turbulent viscosity is higher compared to laminar viscosity [27].
- μ_{eff} : the effective viscosity of the air ($\text{kg} \cdot \text{m}^{-1} \text{s}^{-1}$).
- S_τ : the source term which depends on the air density. This term is generally taken as equal to 1 [27,28,29,30].

2.2.2 Predicted mean vote and predicted percentage of dissatisfaction evaluation

The *PMV* is an index that aims to predict the mean value of votes of a group of occupants on a seven-point thermal sensation scale in an indoor environment [31]. It has been adopted by national and international standards, e.g., ASHARE 55 and ISO 7730 [32]. In Fanger's model, four environmental parameters (air temperature, air velocity, mean radiant temperature, and relative humidity) and two occupants' parameters (metabolic rate and clothing insulation) are combined in the *PMV* index as shown in Equation (2):

$$\begin{aligned} PMV = & (0.303e^{-0.036M} + 0.028)\{(M - W) - 3.05 \times 10^{-3}(5733 - 6.99(M - W) - p_{air}) \\ & - 0.42[(M - W) - 58.15] - 1.7 \times 10^{-5}M(5867 - p_{air}) - 0.0014M(34 - T_{air}) \\ & - 3.96 \times 10^{-8}f_{cl}[(T_{cl} + 273)^4 - (\bar{T}_r + 273)^4] - f_{cl}h_{cl}(T_{cl} - T_{air})\} \end{aligned} \quad (2)$$

where

- M : the metabolic rate “the rate of production of energy with time” ($\text{W} \cdot \text{m}^{-2}$). In this work, M was taken equal to 1 met (1 met = 58 $\text{W} \cdot \text{m}^{-2}$) which corresponds to a sitting and relaxed occupant [32].
- W : the external work ($\text{W} \cdot \text{m}^{-2}$). In this work W was taken equal to 0 W which corresponds to the external work for sedentary tasks and tasks with low activity [33].
- T_{air} : the average air temperature (°C).
- \bar{T}_r : the mean radiant temperature (°C). \bar{T}_r is “the temperature of a uniform, black enclosure that exchanges the same amount of heat by radiation with the occupant as the actual surroundings” [1]. In this work, \bar{T}_r was calculated using the method described in [31] and ISO 7726 [34] based on the office and the occupants' surfaces temperatures. The mean radiant temperature has a strong influence on thermal comfort assessment. It can be shown, using Equation (2), that an error of 1 °C in the estimation of \bar{T}_r leads to an error of 0.24 in the evaluation of the *PMV*.
- p_{air} : the water vapor partial pressure (Pa) (calculated from relative humidity (*RH*) of 50% as shown in Equation (3):

$$p_{air} = RH \times 10 \times \exp\left(\frac{16.6536 - 4030.183}{T_{air}}\right) \quad (3)$$

- T_{cl} : the clothing surface temperature (°C),
- h_c : the convective heat transfer coefficient ($\text{W} \cdot \text{m}^{-2}$). This parameter was estimated using Equation (4):

$$h_c = \max(2.38 \times (T_{cl} - T_{air})^{0.25}, 12.1 \times \sqrt{v_{air}}) \quad (4)$$

where $v_{air} = \sqrt{U^2 + V^2 + W^2}$, is the air velocity (m/s).

- f_{cl} : the clothing surface area factors. This parameter was estimated using Equation (5):

$$f_{cl} = \begin{cases} 1.00 + 1.290 \times I_{cl} & \text{when } I_{cl} < 0.078 \text{ m}^2\text{K/W} \\ 1.00 + 0.645 \times I_{cl} & \text{when } I_{cl} > 0.078 \text{ m}^2\text{K/W} \end{cases} \quad (5)$$

where $I_{cl} = 0.7 \text{ m}^2\text{KW}^{-1}$, is the thermal resistance of clothing.

Once the PMV is calculated, the PPD index, which gives the percentage of people predicted to experience local discomfort can be estimated using Equation (6):

$$PPD = 100 - 95 \times \exp[-0.03353 \times (PMV)^4 - 0.2179 \times (PMV)^2] \quad (6)$$

In this model, thermal neutrality ($PMV = 0$) corresponds to a minimum dissatisfaction percentage of 5%.

2.2.3 Draft rate evaluation

Many people are very sensitive to air velocities at low activity levels. ASHRAE Standard [1] defines draft as «unwanted local cooling of the body caused by air movement». The draft is a very common cause of occupants' complaints in ventilated and air-conditioned environments, especially at low human activity levels (sitting /standing). The sensation of draft depends on the airflow velocity, turbulence intensity, and air temperature. Sensitivity to draft is great where the skin is not covered by clothing, especially the neck, the head, the ankle, and the leg regions.

In this work, the percentage of people feeling draft or DR (%) was estimated using Equation (7):

$$DR = (34 - T_{air}) \times (v_{air} - 0.05)^{0.6223} \times (3.143 + 0.3696 \times v_{air} \times I) \quad (7)$$

where I represents the turbulence intensity (%).

For $v_{air} < 0.05 \text{ m/s}$, we consider $v_{air} = 0.05 \text{ m/s}$ [4], and for $DR > 100\%$, we consider $DR = 100\%$.

As reported in ISO 7730 standard [35], according to the minimum and maximum values of PPD and DR indices, thermal comfort can be classified into the three categories presented in Table 1:

Table 1. Categories of the thermal environment.

Category	PPD (%)	DR (%)
A	$PPD < 6$	$DR < 10$
B	$6 < PPD < 10$	$10 < DR < 20$
C	$10 < PPD < 15$	$20 < DR < 30$
Out	$15 < PPD$	

2.3 Boundary conditions

Table 2 gives the boundary conditions applied in the present work. The value of the occupant's surfaces temperature was based on the experimental work of Liu et al. [36]. This temperature is an important parameter reflecting the human response to cold or thermal stimulus, and states of heat exchange between the human body and the thermal environment.

Table 2. Boundary conditions applied in the present work.

Boundaries	Supply flow rate Q_s (m ³ /h)	50	100	200	300

Inlet	Velocity (m/s)	0.69	1.38	2.76	4.15
	Turbulence intensity (%)	5.26	4.82	4.42	4.20
	MAA (s)	0			
	Temperature (°C)	14			
Outlet	Static pressure (Pa)	0			
	Turbulence intensity (%)	5.06	4.64	4.25	4.04
	MAA (s)	Zero streamwise gradient			
Ceiling, side walls, floor	Velocity (m/s)	No slip			
	MAA (s)	Zero streamwise gradient			
	Temperature (°C)	24			
Occupant	Velocity (m/s)	No slip			
	MAA (s)	Zero streamwise gradient			
	Temperature (°C)	32			
Diffuser, lobed inserts, tube	Velocity (m/s)	No slip			
	MAA (s)	Zero streamwise gradient			
	Heat Flux (W/m ²)	0			

2.4 Grid independence and code validation

The CD case with a supply flow rate $Q_s = 200 \text{ m}^3/\text{h}$ was selected to establish the grid independence and the code validation studies. The grid independence study was conducted with three mesh resolutions. The coarse mesh featured a total of ~ 8 million cells. The finest and medium meshes were obtained by reducing the cell size in the diffuser and the office, resulting in a total of ~ 20 million cells and ~ 13 million cells, respectively.

Figure 4 represents the maximum longitudinal velocity of the jet U_{max} as a function of the horizontal distance d_h from the center of the diffuser (see Figure 5). Accordingly, results with fine and medium mesh are very close, where the maximum percentage error is about 4%, indicating that further refinement which can increase the computational cost, would not bring significant additional accuracy to the solution. As a result, the medium mesh was used for all subsequent simulations.

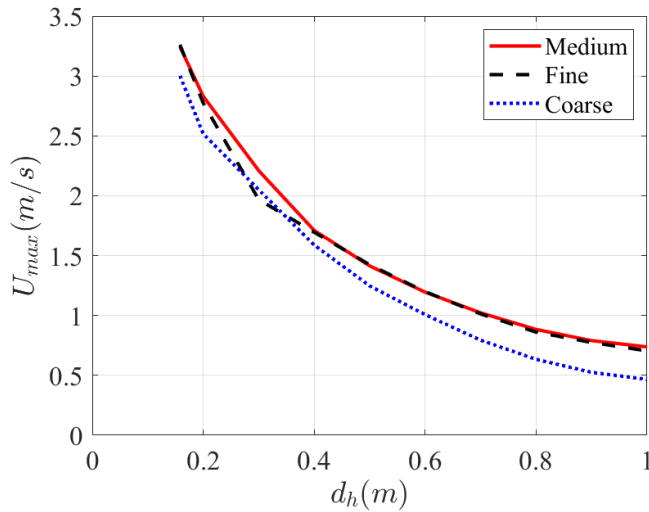


Figure 4. Maximum velocity at different distances from the diffuser for three grid resolutions for $Q_s = 200 \text{ m}^3/\text{h}$.

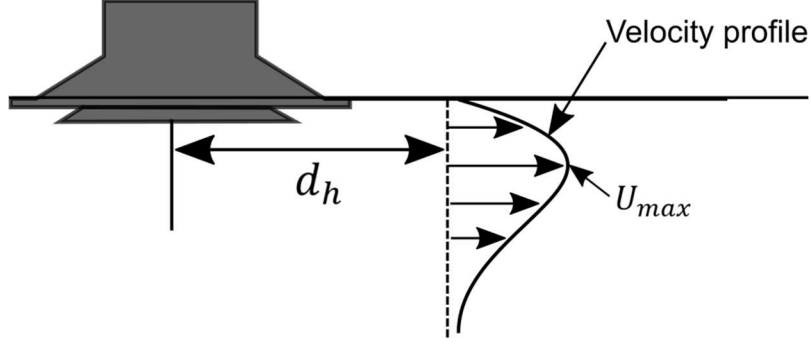


Figure 5. Schematization of the jet velocity profile at a distance d_h from the center of the diffuser.

For the validation process, three different types of turbulence models (named: standard $k-\epsilon$ with enhanced wall treatment, RNG $k-\epsilon$ with enhanced wall treatment, and $k-\omega$ SST), are investigated. A comparison between CFD results and the experimental data of Bragança et al. [18] is performed. Figure 6 represents the predicted maximum jet velocity \hat{v} evolution as a function of a dimensionless distance \hat{R} (see Equation (8)):

$$\hat{R} = \sqrt{\frac{d_h(d_h - R_0)}{R_0 \cdot S_{outer} \cdot \cos(\phi)}}, \quad \hat{v} = \frac{|U_{max}|}{V_n}, \quad (8)$$

where R_0 is the horizontal distance between the neck centerline of the diffuser and its outer trailing edge, ϕ the deflection angle. $V_n = Q_s/A_n$ represents the diffuser neck velocity (m/s), where Q_s is the corresponding supply rate (m^3/s), and A_n is the diffuser neck area (m^2).

According to Figure 6, the $k-\omega$ SST model provides the best agreement and accuracy against the experimental data. Hence, the $k-\omega$ SST model has been chosen to conduct the simulations.

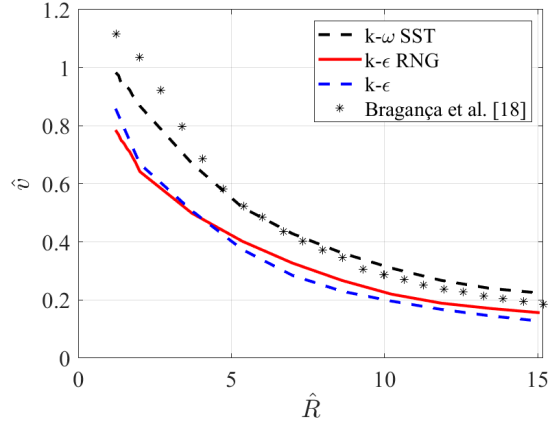


Figure 6. Comparison of the predicted velocity \hat{v} with three different turbulence models and measured data of [18] for $Q_s = 200 \text{ m}^3/\text{h}$.

Table 3 gives the averages of temperature at the outlet, and the averages of mean radiant temperature in the occupied zone compared with those of [18] for two flow rates. Accordingly, a good agreement between CFD and experimental result in both CD and CDLI cases is observed for $Q_s = 200 \text{ m}^3/\text{h}$. However, the results are slightly different for $Q_s = 300 \text{ m}^3/\text{h}$. This can be explained by the difference between the two approaches in setting boundary conditions. In the numerical approach, all surfaces' temperatures are imposed (see Table 2), which allows the comparison between the different cases. However, in the experimental study, surface temperatures were not identical in the different cases (this was deduced from the fact that the mean radiant temperatures are not identical), which makes it difficult to compare the results.

Table 3. Air temperature at the outlet and mean radiant temperature in the occupied zone of the present study compared to those of [18].

200 (m^3/h)				300 (m^3/h)			
CD [18]	CDLI [18]	CD CFD	CDLI CFD	CD [18]	CDLI [18]	CD CFD	CDLI CFD
$T_a (\text{ }^\circ\text{C})$	23.4 ± 0.5	23.8 ± 0.4	23.53	23.44	22.3 ± 0.4	22.3 ± 0.4	23.52
$\bar{T}_r (\text{ }^\circ\text{C})$	24.3 ± 0.8	25.6 ± 0.7	24.26	24.26	23.2 ± 0.7	23.2 ± 0.8	24.26

3. Results and Discussion

3.1 Airflow patterns

In the present study, the airflow field was investigated first, then the *MAA*, *PPD* and *DR* indices were addressed. In a first step, a qualitative comparison was conducted to show the characteristics of the jet at the diffuser exit, and the influence of the lobed inserts on the latter. Figures 7(a-b) show the isosurfaces of velocity magnitude 2 m/s for CD and CDLI cases. This value was chosen to show the expansion of the jet in the zone close to the diffuser. The figures illustrate clearly how the lobed inserts separate the jet inside the diffuser.

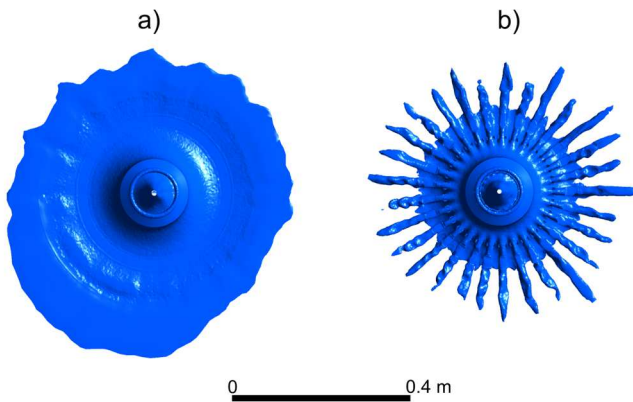


Figure 7. Velocity magnitude (2 m/s) isosurfaces inside and near the diffuser for $Q_s = 200 \text{ m}^3/\text{h}$: a) CD case, b) CDLI case.

The pressure loss through the diffuser is an important parameter of the energy consumption in the distribution system. In order to evaluate this parameter, the pressure was estimated between two points: upstream the diffuser, and in the occupied zone outside the jet region. Figure 8 shows the diffuser's pressure loss for the CD and the CDLI cases with different supply flow rates. Accordingly, the agreement with the experimental data is quite good except for $Q_s = 300 \text{ m}^3/\text{h}$. It can be seen from the figure that the lobed inserts led to a slight increase of pressure loss in the diffuser, which was caused by the reduction of the cross-section. Additionally, the pressure loss in the two cases increases with the supply flow rate.

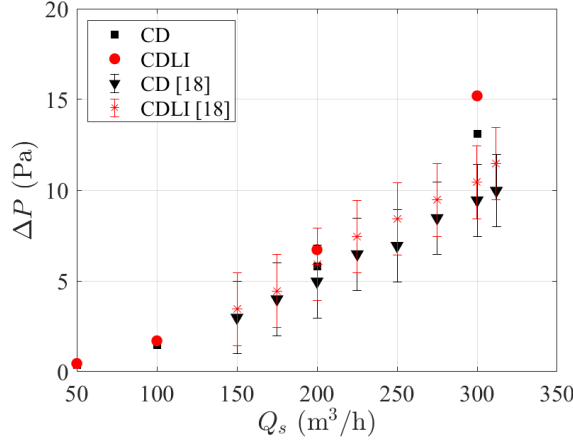


Figure 8. Pressure loss in the diffuser for different supply flow rates compared to data from [18].

Figures 9(a-b) display airflow patterns inside and in the vicinity of the diffuser in the CD and the CDLI cases for $Q_s = 200 \text{ m}^3/\text{h}$. It is shown herein that the flow issuing from the tube is accelerated in the region between the two cones of the diffuser to reach a maximum value which is higher in the CDLI case (see Table 4). According to Figure 9, three recirculation zones are formed inside the diffuser (two zones between the cones and one zone in the center of the diffuser). An additional recirculation zone is created in the CDLI case between the lobed inserts and the diffuser, which may be the cause of the additional pressure loss discussed above. These structures are very important in the near-field mixing [37]. The two jets coming out of each side of the diffuser meet at the outlet of the latter and form one translating jet. The latter is 1.25 times larger in the CDLI case than in the CD case. Since the diffuser has a good Coanda effect, the supply airflow from each diffuser remains attached to the ceiling. Therefore, the temperature in the occupied zone will not be directly affected by the supplied air. It can also be noted that in the CDLI case, the flow detaches at the outlet of the diffuser, and then, it reattaches quickly to the ceiling. This can be explained by the presence of a low-pressure vortex that accentuates the initial pressure difference on both sides of the jet.

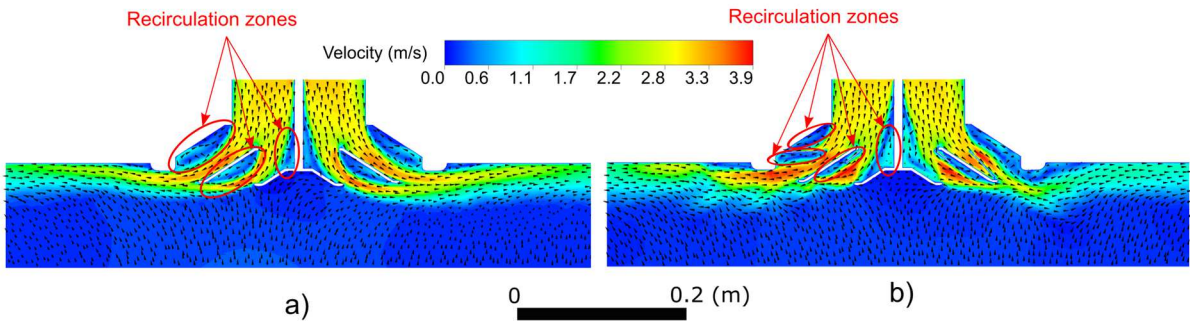


Figure 9. Air velocity magnitude fields and vectors in the near diffuser region in the half middle cross-section of the office for $Q_s = 200 \text{ m}^3/\text{h}$: a) CD case, b) CDLI case.

Table 4. Maximum velocity in the CD and CDLI cases for four supply flow rates.

Q_s (m^3/h)	50	100	200	300
U_{max} (m/s) CD	0.95	1.86	3.70	5.55
U_{max} (m/s) CDLI	1.03	2.04	4.08	6.28

Figure 10 represents the predicted maximum jet velocity U_{max} evolution as a function of the distance d_h for CD and CDLI cases. As it can be seen, the U_{max} profile of the CDLI case decreases faster

compared to that of the CD case. Indeed, near the diffuser ($d_h = 0.15$ m), the difference between the two profiles is about 40%. This difference decreases progressively as a function of the distance from the diffuser until reaching 20% at $d_h = 1$ m.

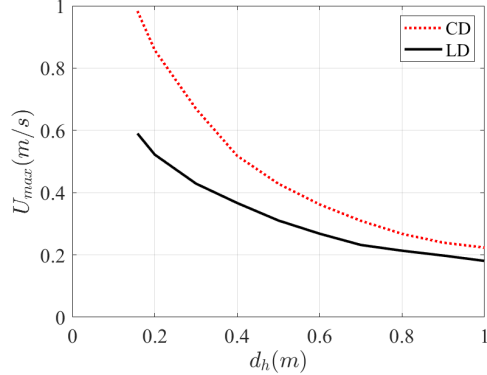


Figure 10. Comparison of the maximum velocity at different distances from the diffuser for CD and CDLI cases for $Q_s = 200$ m^3/h .

The flow patterns could be used primarily as an indicator of the depth of fresh air penetration in the occupied zone. Figures 11-12 provide the airflow in the half middle cross-sections ($Z = 0$ m and $X = 1.735$ m, respectively) of the office and streamlines near the diffuser for the CD and the CDLI cases for $Q_s = 200$ m^3/h . First, we notice that the flow has a radial distribution when it leaves the diffusers in both CD and CDLI cases. Second, in both cases, the airflow from the diffuser's openings translates throughout the ceiling before reaching the sidewalls of the office. Since the impact is in the corner of the office room and the sidewalls are vertical, a downhill flow is generated. The latter spreads downward along the side walls as a wall jet, where it will be accelerated by the effect of reverse buoyancy. The jets will then be separated from the vertical walls due to the upward convection current generated near the latter. Consequently, flow recirculation zones (marked with solid red arrows) are formed near each wall. Those recirculation zones are related to the existence of two parallel flows: the downward jet, and the upward flow above the occupant (marked with red dashed arrows). The latter results from the combination of: (1) the occupant's plume driven by the temperature difference between the warm occupant and colder ambient air, (2) the aspiration caused by the diffuser. It should be noted that these structures are responsible for mixing the air inside the office. This result revealed the interaction between the ambient flow generated primarily by the ventilation system and the occupant's plume. This interaction affects the final flow pattern in the occupied zone [38, 39] thereby, influencing the thermal comfort level and the air quality.

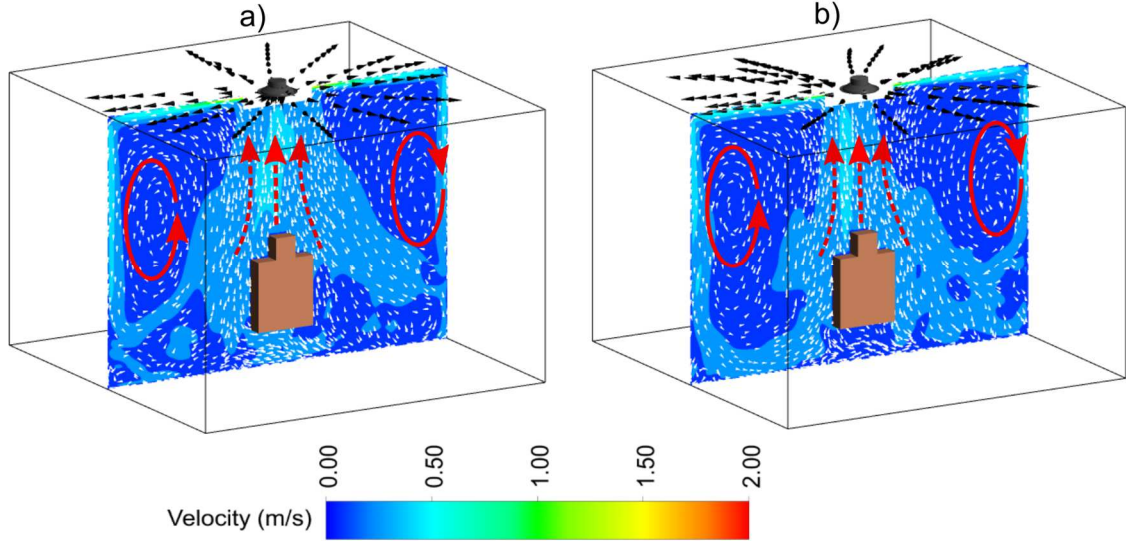


Figure 11. Velocity magnitude distribution in the half middle cross-section ($Z = 0$ m) of the office and velocity streamlines near the diffuser for $Q_s = 200 \text{ m}^3/\text{h}$: a) CD case, b) CDLI case.

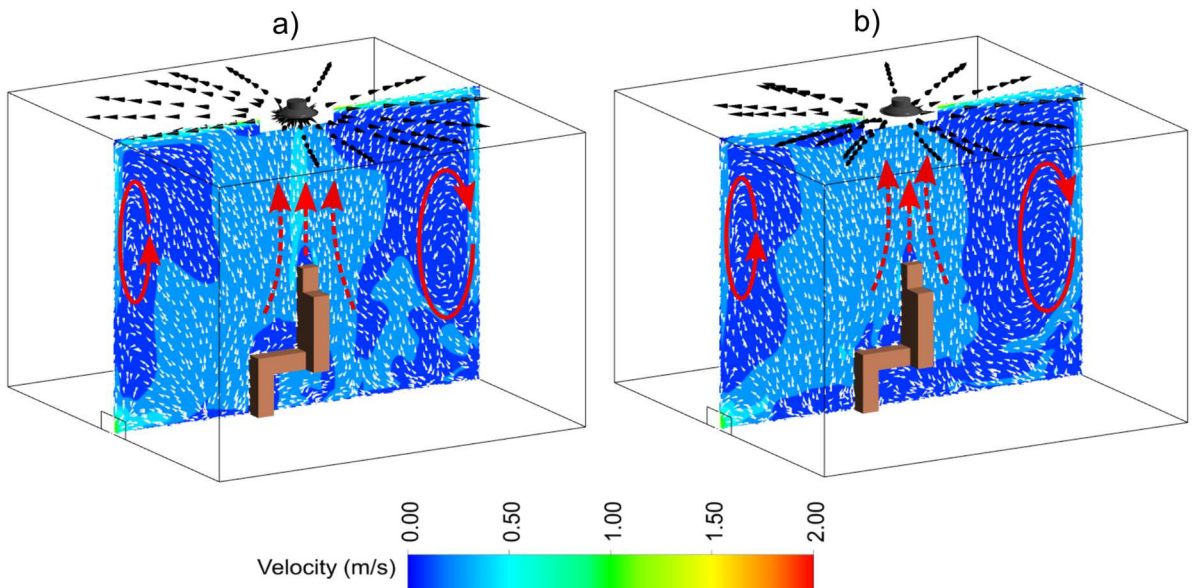


Figure 12. Velocity magnitude distribution in the half middle cross-section ($X = 1.735$ m) of the office and velocity streamlines near the diffuser for $Q_s = 200 \text{ m}^3/\text{h}$: a) CD, b) CDLI.

Figures 13(a-b) show the velocity and temperature profiles of the occupant's plume at three different heights. Accordingly, close to the occupant's head, high temperatures and low velocities occur. Identical trends were recorded in previous works conducted by Quintela, [40] using surface-mounted cubes and later by Borges et al. [41] using a thermal manikin. Quintela, [40] suggested that separation of flows may occur above the occupant's head, resulting in a particular dead air region. Moreover, the velocity and temperature profiles of the CD case are shifted and slightly higher than those of the CDLI case. This may result from the aspiration caused by the Coanda effect which is slightly higher in the CD case as it is shown in Figure 10.

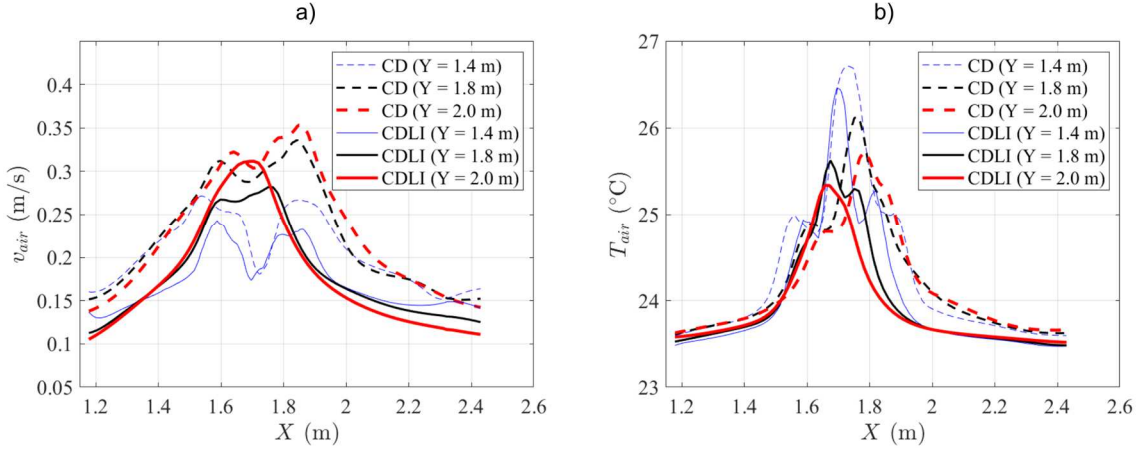


Figure 13. a) Velocity profiles of the plume generated by the occupant in CD and CDLI cases, b) temperature profiles of the plume generated by the occupant in CD and CDLI cases.

3.2 Temperature

The two horizontal XZ planes located at vertical distances $y = 0.1$ m and $y = 1.1$ m from the ground were considered to evaluate the temperature. The two planes are located at the level of the occupant's head and foot. Figures 14-17 show contours of air temperature in the two horizontal XZ planes for the two considered cases and the four supply flow rates. According to the presented fields, the temperature is nearly uniform in all planes with average values ranging between 23 °C and 24 °C (see Table 5), except in the vicinity of the occupant and the heated walls where a large temperature gradient was observed. This can be explained by the fact that the cold wall jet flows were heated by the hot surfaces before being mixed with the ambient air. Depending on the supply flow rate, the supplied air can reach the occupied zone at different temperatures.

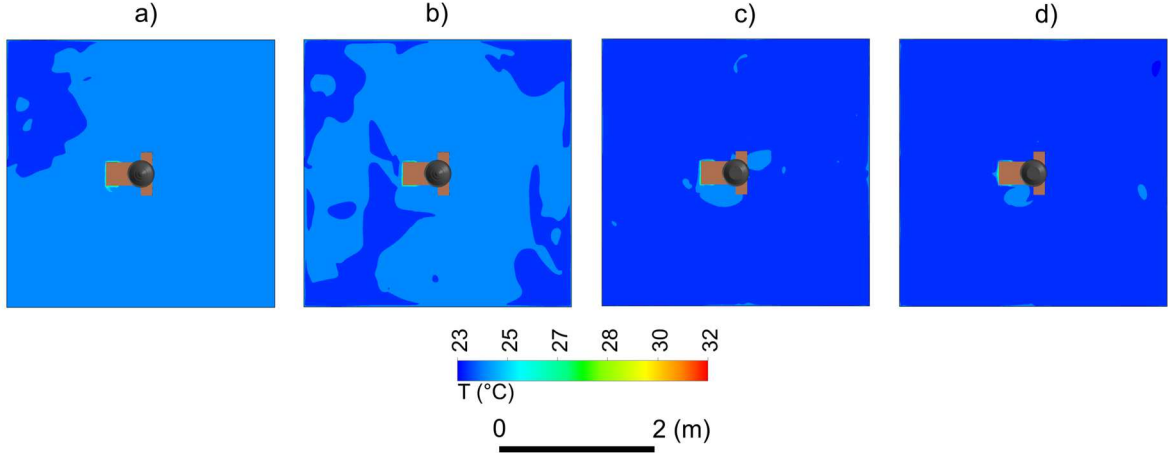


Figure 14. Air temperature distributions in the plane $y = 0.1$ m for CD case for: a) $Q_s = 50 \text{ m}^3/\text{h}$, b) $Q_s = 100 \text{ m}^3/\text{h}$, c) $Q_s = 200 \text{ m}^3/\text{h}$, d) $Q_s = 300 \text{ m}^3/\text{h}$.

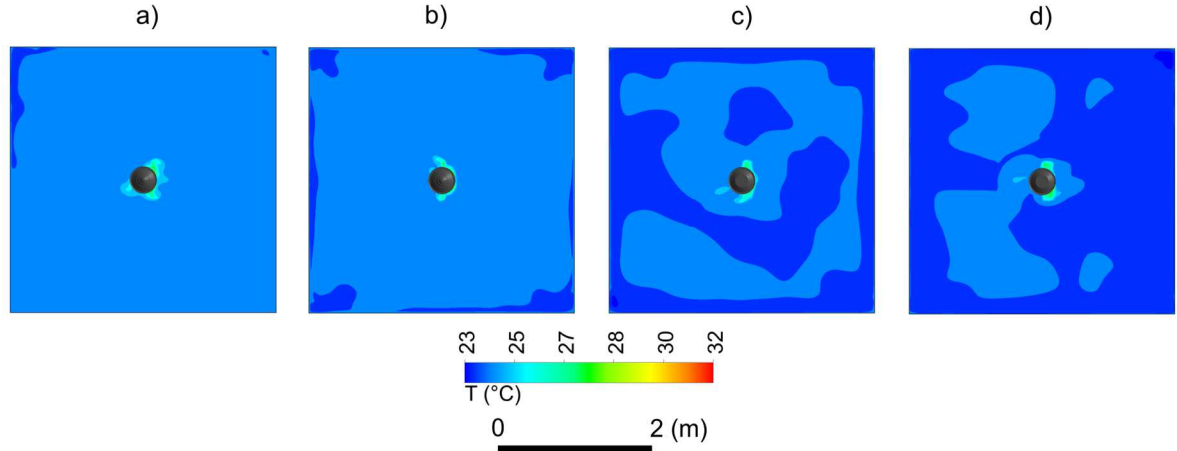


Figure 15. Air temperature distributions in the plane $y = 1.1$ m for CD case for: a) $Q_s = 50 \text{ m}^3/\text{h}$, b) $Q_s = 100 \text{ m}^3/\text{h}$, c) $Q_s = 200 \text{ m}^3/\text{h}$, d) $Q_s = 300 \text{ m}^3/\text{h}$.

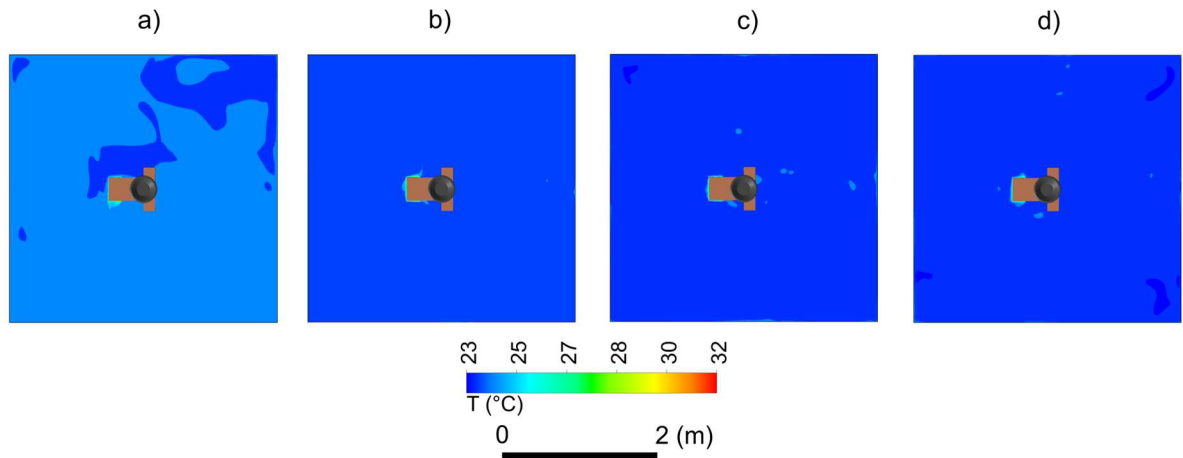


Figure 16. Air temperature distributions in the plane $y = 0.1$ m for CDLI case for: a) $Q_s = 50 \text{ m}^3/\text{h}$, b) $Q_s = 100 \text{ m}^3/\text{h}$, c) $Q_s = 200 \text{ m}^3/\text{h}$, d) $Q_s = 300 \text{ m}^3/\text{h}$.

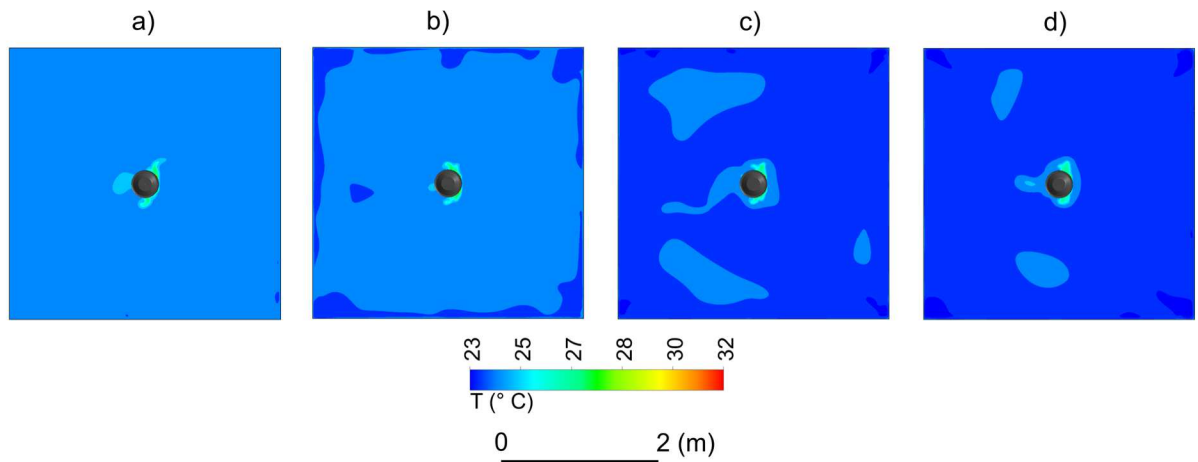


Figure 17. Air temperature distributions in the plane $y = 1.1$ m for CDLI case for: a) $Q_s = 50 \text{ m}^3/\text{h}$, b) $Q_s = 100 \text{ m}^3/\text{h}$, c) $Q_s = 200 \text{ m}^3/\text{h}$, d) $Q_s = 300 \text{ m}^3/\text{h}$.

Table 5. Average air temperature in the two planes $y = 0.1$ m and $y = 1.1$ m for CD and CDLI cases and different supply flow rates.

$Q_s (\text{m}^3/\text{h})$	CD		CDLI	
	$y = 0.1$ m	$y = 1.1$ m	$y = 0.1$ m	$y = 1.1$ m

50	23.85	24.03	23.81	24.02
100	23.75	23.88	23.71	23.86
200	23.58	23.78	23.47	23.66
300	23.48	23.70	23.36	23.59

3.3 Comfort indicators

Table 6 shows the statistics of *DR* and *PPD* indices for the CD and the CDLI cases, and for two supply rates compared to those of [18]. In terms of *DR*, the trends of the CFD results correspond to the experimental data with some differences between the estimated levels, which are probably due to numerical and experimental errors. According to the table, for $Q_s = 200 \text{ m}^3/\text{h}$, the CFD predicts 79% and 80% of the points in category A against 21% and 20% in category B for the CD and the CDLI cases, respectively. For $Q_s = 300 \text{ m}^3/\text{h}$, 55% and 63% of the points are in category A against 45% and 35% in category B for the CD and the CDLI cases, respectively. 2% of the points are in category C for the CDLI case.

In terms of *PPD*, the CFD predicted an identical thermal comfort level for both diffusers for $Q_s = 200 \text{ m}^3/\text{h}$; 92% of the points in category A, 7% between category B and category C, and 1% where the *PPD* is higher than 15%. However, the experimental study showed a clear improvement in *PPD* in the CDLI case. For $Q_s = 300 \text{ m}^3/\text{h}$, the CFD shows that 78% and 75% of the points are in category A, 32% and 22% in category B for the CD and the CDLI cases, respectively. 3% of the points are in category C in the CDLI case. The experiment predicted no points in category A. As discussed above, the differences between the comfort levels estimated by the CFD and the experiment is probably due to the mean radiant temperatures. Indeed, contrary to the CFD approach, the latter was not controlled accurately in experimental study which may lead to an overestimation or underestimation of the comfort.

Table 6. Statistic distribution of *PPD* and *DR* indices using 64 points, for the two cases and two supply flow rates compared to those of [18].

		200 m ³ /h				300 m ³ /h			
		CD		CDLI		CD		CDLI	
		[18]	CFD	[18]	CFD	[18]	CFD	[18]	CFD
A	<i>DR</i> < 10	98	79	100	80	53	55	87	63
B	10 < <i>DR</i> < 20	2	21	0	20	47	45	13	35
C	20 < <i>DR</i> < 30	0	0	0	0	0	0	0	2
A	<i>PPD</i> < 6	81	92	100	92	0	68	0	75
B	6 < <i>PPD</i> < 10	19	6	0	6	31	32	78	22
C	10 < <i>PPD</i> < 15	0	1	0	1	31	0	8	3
Out	15 < <i>PPD</i>	0	1	0	1	38	0	4	0

To confirm the trends of this statistical study, and since the CFD allows post-processing a large number of points, another study was performed using 12000 points distributed randomly in the occupied zone. The results are presented in Table 7 for the four flow rates. First, there is an increase in the number of points in category A of the *PPD* and the *DR*, however, the differences between the comfort levels of the CD and the CDLI remain identical to those obtained with 64 points. Second, in terms of *DR*, 100% of the points are in category A for flow rates $Q_s = 50 \text{ m}^3/\text{h}$ and $Q_s = 100 \text{ m}^3/\text{h}$ in both CD and CDLI cases. Then, when Q_s exceeded $100 \text{ m}^3/\text{h}$, the relatively high supply flow rate resulted in a certain dissatisfaction in the occupied zone with an advantage for the CDLI case. This improvement is larger for $Q_s = 300 \text{ m}^3/\text{h}$. Finally, in terms of *PPD*, results are interesting since they show an improvement in thermal comfort in relation to flow rate between $Q_s = 50 \text{ m}^3/\text{h}$ and $Q_s = 200 \text{ m}^3/\text{h}$. The comfort deteriorates slightly for $Q_s = 300 \text{ m}^3/\text{h}$ because the heat exchanges between the

heated walls and the high-velocity wall jet are low. Consequently, the air reaches the occupied zone with a low temperature. It can be noted that for $Q_s = 50 \text{ m}^3/\text{h}$, a very important improvement has been provided by the lobed inserts.

Table 7. Statistic distribution of *PPD* and *DR* indices using 12000 points, randomly distributed in the occupied zone, for the CD and CDLI cases and four supply flow rates.

Flow rates (m^3/h)	50		100		200		300	
	CD	CDLI	CD	CDLI	CD	CDLI	CD	CDLI
A $DR < 10$	100	100	100	100	92	94	66	72
B $10 < DR < 20$	0	0	0	0	8	6	34	28
C $20 < DR < 30$	0	0	0	0	0	0	0	0
A $PPD < 6$	27	47	95	100	100	100	91	93
B $6 < PPD < 10$	73	53	5	0	0	0	9	7
C $10 < PPD < 15$	0	0	0	0	0	0	0	0
Out $15 < PPD$	0	0	0	0	0	0	0	0

3.4 Air freshness

Table 8 presents the average values of *MAA* in the breathing zone (a $0.2 \text{ cm} \times 0.2 \text{ cm} \times 0.2 \text{ cm}$ cubature was assumed to be in front of the occupant's head) for four supply flow rates. First, we notice an obvious decrease in the *MAA* when the airflow rate increases for both CD and CDLI cases. Second, a deterioration of the air freshness caused by the lobed inserts is clearly visible with supply flow rates of $200 \text{ m}^3/\text{h}$ and $100 \text{ m}^3/\text{h}$. For $Q_s = 50 \text{ m}^3/\text{h}$, the *MAA* is larger in the CD case than that in the CDLI case. Finally, for $Q_s = 300 \text{ m}^3/\text{h}$, the difference of *MAA* between the CD and the CDLI cases is not significant.

Table 8. Average values of *MMA* in the breathing zone for four supply flow rates.

$Q_s (\text{m}^3/\text{h})$	50	100	200	300
<i>MAA</i> (s) CD	197.66	144.80	76.73	59.95
<i>MAA</i> (s) CDLI	186.77	153.19	85.21	59.58

Figures 18-19 show the *MAA* contours in the office room for the CD and the CDLI cases and different flow rates at $y = 1.1 \text{ m}$. Accordingly, for both CD and CDLI cases, the maximum *MAA* at the head level decreases with increasing flow rate. On the other hand, the areas with higher *MAA* values are larger in the CDLI case than that in the CD case for the different flow rates. This is probably due to the thermal plume, which has slightly higher velocities in the CD case compared to the CDLI case (see Figure 13 (a)). This result confirms the previous one obtained with the average values (see Table 8). In addition, in both CD and CDLI cases, the *MMA* values in the region behind the occupant were significantly higher than those in front of the occupant. This is due to the air confinement and the formation of vortices in this area, which increases the air residence time.

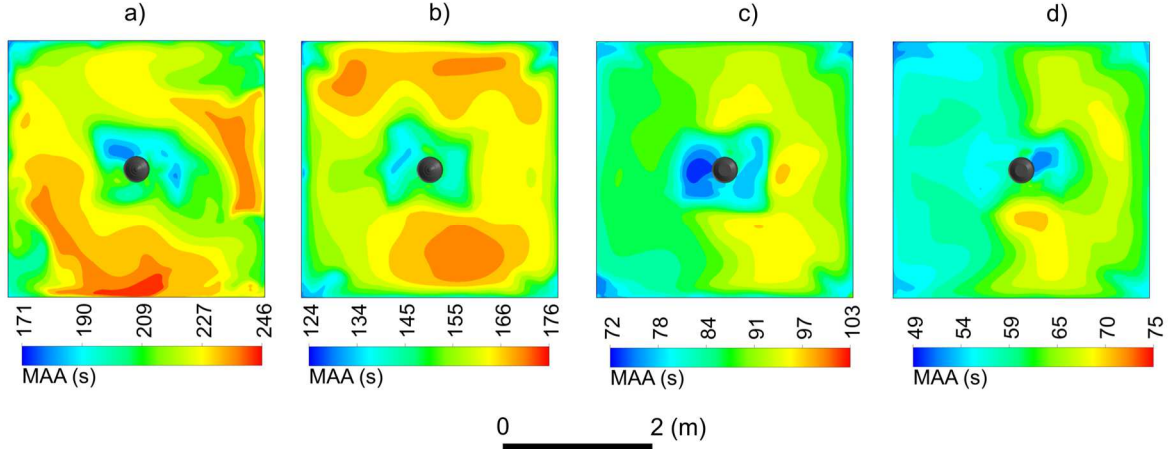


Figure 18. *MAA* distributions at the head level ($y = 1.1$ m) in the CD case for: a) $Q_s = 50$ m^3/h , b) $Q_s = 100$ m^3/h , c) $Q_s = 200$ m^3/h , d) $Q_s = 300$ m^3/h .

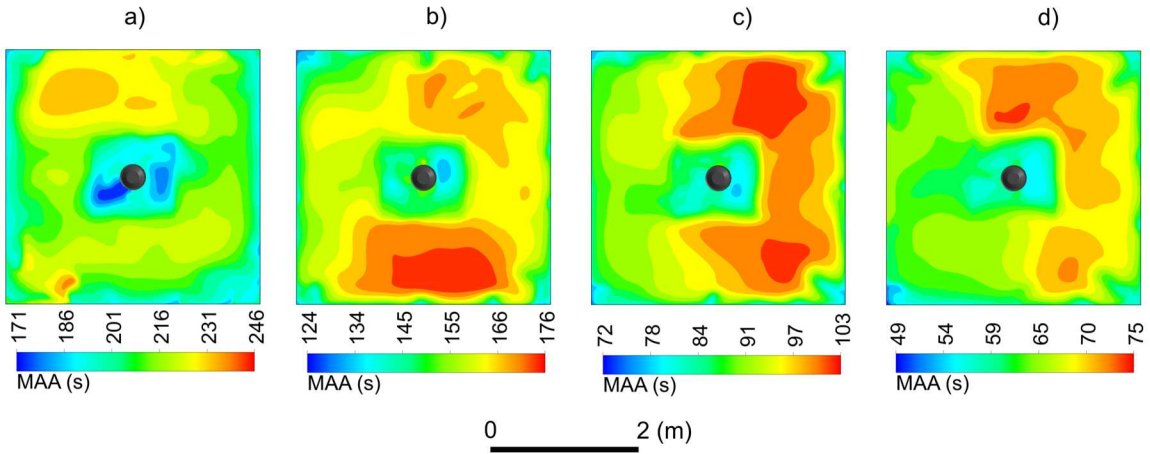


Figure 19. *MAA* distributions at the head level ($y = 1.1$ m) in the CDLI case for: a) $Q_s = 50$ m^3/h , b) $Q_s = 100$ m^3/h , c) $Q_s = 200$ m^3/h , d) $Q_s = 300$ m^3/h .

4. Conclusions

In the present work, numerical simulations were conducted using Ansys Fluent software to study the thermal comfort and air freshness in an office room. Two cases were considered: a first case with a ceiling round diffuser (assigned as CD), and a second case with the same diffuser equipped with lobed inserts (CDLI case). The simulations were performed with several supply air rates. A user-defined scalar and user-defined function were used to solve the mean age of air (*MAA*), and thermal comfort indices (*PPD*, *DR*) equations, respectively. A good agreement was found between the CFD results and the experimental data.

The analysis shows that the flow exits from the diffuser as a jet attached to the ceiling and slides along the latter. This jet is 1.25 times larger in the CDLI case compared to the CD case. A statistical analysis over 12000 points - distributed randomly in the occupied zone - revealed that lobed inserts can reduce thermal dissatisfaction and draft effect in the occupied zone. This thermal comfort enhancement depends on the supply flow rate. Indeed, for flow rates $Q_s = 50$ m^3/h and $Q_s = 100$ m^3/h , the draft effect in the occupied zone is in category A for both CD and CDLI cases. For flow rates higher than 100 m^3/h , the draft effect increases in the occupied zone. In these conditions, it has been shown that the lobed inserts reduce the draft effect, especially for $Q_s = 300$ m^3/h . In terms of *PPD*, an enhancement of thermal comfort was observed as a function of flow rate between $Q_s = 50$ m^3/h and $Q_s = 200$ m^3/h . However, for $Q_s = 300$ m^3/h , the thermal comfort has deteriorated because the heat exchanges between the heated walls and the high velocity wall jet are low. Therefore, the air reaches

the occupied zone with a low temperature. It can be noted that for the case $Q_s = 50 \text{ m}^3/\text{h}$, a very important improvement of thermal comfort has been provided by the lobed inserts.

The analysis of the *MAA* result shows that air freshness increases with the flow rate. At the same time, a slight deterioration in the air freshness was noticed at the level of the occupant's head in the CDLI case. For both CD and CDLI cases, the air is fresher behind the occupant than in the frontal area.

The present work has shown that lobed inserts can improve thermal comfort and draft in an office room for different supply flow rates in cooling mode. Additional works are still needed to show their efficiency in winter conditions with a warm jet. However, improvements in their geometry are still needed to increase their efficiency in terms of air freshness. Further studies can also be conducted to show the effectiveness of lobed inserts in other areas such as a car cabin.

The simulations conducted in this work, correspond to simplistic conditions where only one occupant is present in the middle of the office. Therefore, it is necessary to perform simulations in more realistic environments with the presence of furniture and/or several occupants.

Declaration of competing interest

The authors declare that they have no known competing financial interests or personal relationships that could have appeared to influence the work reported in this paper.

References

- [1] ASHRAE, « Thermal environmental conditions for human occupancy ANSI-ASHRAE, Standard ASHRAE 55-1992 », 1992.
- [2] D. Müller, C. Kandzia, A. Melikov, et P. Nielson, *Mixing ventilation: Guide on mixing air distribution design*. REHVA: Federation of European Heating and Air-conditioning Associations. 2013.
- [3] K. Adalberth, « Energy use during the life cycle of single-unit dwellings: Examples », *Build. Environ.*, vol. 32, n° 4, p. 321-329, juill. 1997, doi: 10.1016/S0360-1323(96)00069-8.
- [4] H. D. Goodfellow et E. Tahti, *Industrial ventilation design guidebook*, Academic press. 2001.
- [5] H. B. Awbi, *Ventilation of buildings*, Routledge. 2002.
- [6] NF EN 16798, « Energy performance of buildings. », 2017.
- [7] P. V. Nielsen, T. Heby, et B. Moeller-Jensen, « Air Distribution in a Room with Ceiling-Mounted Diffusers--Comparison with Wall-Mounted Diffuser, Vertical Ventilation, and Displacement Ventilation », *ASHRAE Trans.*, vol. 112(2), 2006.
- [8] Y. K. Chuah, S. C. Hu, et J. M. Barber, « Airflow characteristics of circular ceiling diffusers. International Journal on Architectural Science, 1, 59-67. », *Int. J. Archit. Sci.*, vol. 1, p. 59-67, 2000.
- [9] S. Shakerin et P. L. Miller, « Experimental study of vortex diffusers », NREL/TP-472-7331, 137437, nov. 1995. doi: 10.2172/137437.
- [10] S. C. Hu, « Airflow characteristics in the outlet region of a vortex room air diffuser », *Build. Environ.*, vol. 38, n° 4, p. 553-561, avr. 2003, doi: 10.1016/S0360-1323(02)00187-7.
- [11] M. A. Aziz, I. A. M. Gad, E. S. F. A. Mohammed, et R. H. Mohammed, « Experimental and numerical study of influence of air ceiling diffusers on room air flow characteristics », *Energy Build.*, vol. 55, p. 738-746, déc. 2012, doi: 10.1016/j.enbuild.2012.09.027.

- [12] B. Sajadi, M. H. Saidi, et A. Mohebbian, « Numerical investigation of the swirling air diffuser: Parametric study and optimization », *Energy Build.*, vol. 43, n° 6, p. 1329-1333, juin 2011, doi: 10.1016/j.enbuild.2011.01.018.
- [13] A. Kuchar et R. Chamberlin, « Scale model performance test investigation of exhaust system mixers for an Energy Efficient Engine /E3/ propulsion system », présenté à 18th Aerospace Sciences Meeting, Pasadena, CA, U.S.A., janv. 1980. doi: 10.2514/6.1980-229.
- [14] W. Presz, Jr., G. Reynolds, et D. McCormick, « Thrust augmentation using mixer-ejector-diffuser systems », présenté à 32nd Aerospace Sciences Meeting and Exhibit, Reno, NV, U.S.A., janv. 1994. doi: 10.2514/6.1994-20.
- [15] G. Power, M. McClure, et D. Vinh, « Advanced IR suppressor design using a combined CFD/test approach », présenté à 30th Joint Propulsion Conference and Exhibit, Indianapolis, IN, U.S.A., juin 1994. doi: 10.2514/6.1994-3215.
- [16] H. Hu, T. Kobayashi, T. Saga, N. Taniguchi, H. Liu, et S. Wu, « Research on the rectangular lobed exhaust ejector/mixer systems », *Transactions-Japan society for aeronautical and space sciences*, p. 187-194, 1999.
- [17] I. Nastase, A. Meslem, I. Vlad, et I. Colda, « Lobed grilles for high mixing ventilation – An experimental analysis in a full scale model room », *Build. Environ.*, vol. 46, n° 3, p. 547-555, mars 2011, doi: 10.1016/j.buildenv.2010.08.008.
- [18] P. Bragança, K. Sodjavi, A. Meslem, et L. Serres, « Airflow characteristics and thermal comfort generated by a multi-cone ceiling diffuser with and without inserted lobes », *Build. Environ.*, vol. 108, p. 143-158, nov. 2016, doi: 10.1016/j.buildenv.2016.08.029.
- [19] P. Bragança, K. Sodjavi, A. Meslem, et I. Nastase, « Passive control strategy for mixing ventilation in heating mode using lobed inserts », *Energy Build.*, vol. 133, p. 512-528, déc. 2016, doi: 10.1016/j.enbuild.2016.10.023.
- [20] M. Fan *et al.*, « A review of different ventilation modes on thermal comfort, air quality and virus spread control », *Build. Environ.*, vol. 212, p. 108831, mars 2022, doi: 10.1016/j.buildenv.2022.108831.
- [21] J. L. Domingo, M. Marquès, et J. Rovira, « Influence of airborne transmission of SARS-CoV-2 on COVID-19 pandemic. A review », *Environ. Res.*, vol. 188, p. 109861, sept. 2020, doi: 10.1016/j.envres.2020.109861.
- [22] C. Topp, P. Hesselholt, M. R. Trier, et P. V. Nielsen, « Influence of geometry of thermal manikins on room airflow », 2003, p. 339-344.
- [23] D. Zukowska, A. Melikov, et Z. Popolek, « Thermal plume above a simulated sitting person with different complexity of body geometry. In Proceedings of the 10th International Conference on Air Distribution in Rooms », Technical University of Denmark, 2007, p. 191-198.
- [24] M. W. Simons et J. R. Walter, « Ventilation effectiveness parameters resulting from mechanical ventilation with recirculation », 2002.
- [25] L. Davidson et E. Olsson, « Calculation of age and local purging flow rate in rooms », *Build. Environ.*, vol. 22, n° 2, p. 111-127, janv. 1987, doi: 10.1016/0360-1323(87)90031-X.
- [26] ANSYS Inc. (2020). ANSYS FLUENT 12.0/12.1 Documentation.

- [27] V. Chanteloup et P.-S. Mirade, « Computational fluid dynamics (CFD) modelling of local mean age of air distribution in forced-ventilation food plants », *J. Food Eng.*, vol. 90, n° 1, p. 90-103, janv. 2009, doi: 10.1016/j.jfoodeng.2008.06.014.
- [28] G. Gan, « Effective depth of fresh air distribution in rooms with single-sided natural ventilation », *Energy Build.*, vol. 31, n° 1, p. 65-73, janv. 2000, doi: 10.1016/S0378-7788(99)00006-7.
- [29] M. Bartak *et al.*, « Integrating CFD and building simulation », *Build. Environ.*, vol. 37, n° 8-9, p. 865-871, août 2002, doi: 10.1016/S0360-1323(02)00045-8.
- [30] S. C. Hu et Y. K. Chuah, « Deterministic simulation and assessment of air-recirculation performance of unidirectional-flow cleanrooms that incorporate age of air concept », *Build. Environ.*, vol. 38, n° 4, p. 563-570, avr. 2003, doi: 10.1016/S0360-1323(02)00072-0.
- [31] P. O. Franger, « Thermal comfort: Analysis and applications in environmental engineering », *Appl. Ergon.*, vol. 3, n° 3, p. 181, sept. 1972, doi: 10.1016/S0003-6870(72)80074-7.
- [32] S. Carlucci, L. Bai, R. de Dear, et L. Yang, « Review of adaptive thermal comfort models in built environmental regulatory documents », *Build. Environ.*, vol. 137, p. 73-89, juin 2018, doi: 10.1016/j.buildenv.2018.03.053.
- [33] G. Havenith, I. Holmér, et K. Parsons, « Personal factors in thermal comfort assessment: clothing properties and metabolic heat production », *Energy Build.*, vol. 34, n° 6, p. 581-591, juill. 2002, doi: 10.1016/S0378-7788(02)00008-7.
- [34] ISO 7726, E. N. « Ergonomics of the Thermal Environment: Instruments for Measuring Physical Quantities », 1998.
- [35] ISO 7730, « Ergonomics of the Thermal Environment - Analytical Determination and Interpretation of Thermal Comfort Using Calculation of the PMV and PPD Indices and Local Thermal Comfort Criteria », 2005.
- [36] W. Liu, Z. Lian, Q. Deng, et Y. Liu, « Evaluation of calculation methods of mean skin temperature for use in thermal comfort study », *Build. Environ.*, vol. 46, n° 2, p. 478-488, févr. 2011, doi: 10.1016/j.buildenv.2010.08.011.
- [37] E. Tavakoli et R. Hosseini, « Large eddy simulation of turbulent flow and mass transfer in far-field of swirl diffusers », *Energy Build.*, vol. 59, p. 194-202, avr. 2013, doi: 10.1016/j.enbuild.2012.12.029.
- [38] Z. Liu, D. Yin, Y. Niu, G. Cao, H. Liu, et L. Wang, « Effect of human thermal plume and ventilation interaction on bacteria-carrying particles diffusion in operating room microenvironment », *Energy Build.*, vol. 254, p. 111573, janv. 2022, doi: 10.1016/j.enbuild.2021.111573.
- [39] P. Peng *et al.*, « Experimental investigation on the ventilation performance of diffuse ceiling ventilation in heating conditions », *Build. Environ.*, vol. 205, p. 108262, nov. 2021, doi: 10.1016/j.buildenv.2021.108262.
- [40] D. A. Quintela, « Thermal convection from a cubic body immersed in a turbulent boundary layer », University of Coimbra, Portugal, 1989.
- [41] C. P. Borges, D. A. Quintela, G. N. Brites, A. R. Gaspar, et J. J. Costa, « Analysis of thermal plumes generated by a seated person, a thermal manikin and a dummy. », présenté à Roomvent, 2002.